Underwater Interaction of 1064 nm Laser Radiation with Metal Target

G. Toker, V. Bulatov, T. Kovalchuk and I. Schechter

Abstract—Dynamics of laser radiation – metal target interaction in water at 1064 nm by applying Mach-Zehnder interference technique was studied. The mechanism of generating the well developed regime of evaporation of a metal surface and a spherical shock wave in water is proposed. Critical intensities of the NIR for the well developed evaporation of silver and gold targets were determined. Dynamics of shock waves was investigated for earlier (dozens) and later (hundreds) nanoseconds of time. Transparent expanding plasma-vapor-compressed water object was visualized and measured. The thickness of compressed layer of water and pressures behind the front of a shock wave for later time delays were obtained from the optical treatment of interferograms.

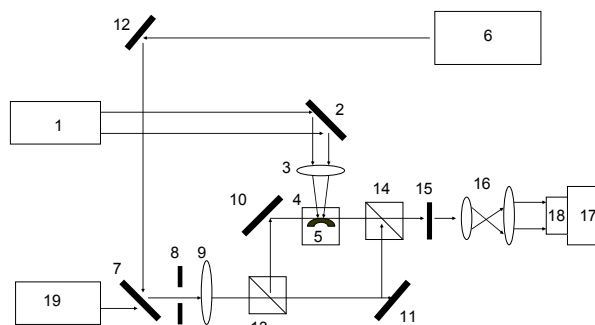*Keywords*—laser, shock wave, metal target, underwater

I. INTRODUCTION

1. Experimental results and discussion

THE underwater interaction of the IR laser radiation with silver and gold targets was investigated for the purpose of understanding processes accompanying treatment of the metal target by *1064* nm laser radiation. Treatment of different types of targets at $\lambda=1064$ nm were studied in [1, 2]; in [3, 4] were investigated processes of generation of nanoparticles; research of interaction of red $\lambda=694.3$ nm radiation with a metal target in water was performed by applying holographic interferometry [5].

1.1. Experimental set-up

The processes of *1064* nm laser radiation interaction with metal targets were visualized and measured by using a Mach-Zehnder interference approach. The scheme of the experiment is presented in Fig.1.

The laser used for underwater interaction with a metal target was a Nd:YAG laser (Continuum, Powerlite-8010, US). Its basic harmonic pulses *(λ = 1064* nm, duration *6* ns) were focused by a singlet (of *75* mm focal length) into a quartz-windowed cuvette, where a metal target was located. The maximal output energy was reduced down to ~ 100 mJ. The focal spot diameter was of ~ 50 μm. The laser beam intensity was varied in the range: *0.085–0.85* GW.cm^{-2}.

All authors are with the Israel Institute of Technology, Dept. of Chemistry, 32000 Haifa, Israel (correspondent author to provide phone: 972-4-8292638; cell:972-526-273-537; fax:972-4-8295703; e-mail: gtoker@tx.technion.ac.il

1-1064 nm laser; **2**-1064 mirror; **3**-1064 nm lens; **4**-cuvette; **5**-target; **6**-Ar-ion pilot laser; **7**-beam splitter; **8**-diaphragm; **9**-expanding lens;**10,11,12**-mirrors; **13,14** beam splitting cubes; **15**-532 nm filter; **16**- collimator; **17**-CCD camera;**18** sensor; **19**-532 nm laser

Fig. 1. Experimental set-up

A second laser was used for probing the interaction events, at a controlled time delay: the second harmonic radiation *(λ =532* nm, *6* ns) of a Nd:YAG laser (Quanta-Ray INDI-YAG laser, Spectra Physics, CA) was applied for inspecting the region of study in the direction perpendicular to the light propagation of the first laser beam. Both laser systems operated in single pulse mode and were synchronized by using a pulse generator (BNC 555-8CG, Berkley Nucleonic Corp., Berkley, CA), with accuracy better than *6* ns. The synchronization was used for visualizing the dynamics of the plasma-shock wave object evolution for different controlled time delays between the heating and diagnostic laser pulses.

Mach-Zehnder interference imaging technique was applied for visualizing and measuring the region under investigation. The interferometer consists of two beam splitting cubes and two flat mirrors as it shown in Fig.1. Focusing interferometric photographs were obtained by using an optical collimation system, consisting of two objective lenses: ILOCA-Quinon, $F = 50$ mm and Jupiter-9, $F = 85$ mm. The plasma of breakdown on the surface of a metal target was sharply imaged by the collimator on the sensitive area of the CMOS camera (Alpha-900, Sony). The CMOS camera works in mode of a full-frame (24x36.9 mm^2) sensor with resolution of ~ 6 megapixels (size of the pixel is ~ 12 microns). The method produces an imaging with magnification of ~ 4 μm/pix, coefficient of the magnification $M\sim 3$ and spatial resolution *24* μm. Time delays τ_d were measured between maximums of the laser pulses.

1.2. Interferograms

Sharp focusing of the laser light in a spot of ~ 50 μm diameter produces laser flux of the order $E_{lp} \sim (0.51 \div 5.1) x 10^3$ J.cm^{-2}, leading to generation of high temperature ablation plasma on the surface of a metal target immersed in water. Spherically expanding surface plasma as a piston accelerates a layer of the surrounding liquid. In earlier stages of expansion (dozens of ns) of the ablation plasma a shock wave in water moves with supersonic velocities. The dynamics of the plasma object could be approximated by the model of point explosion [6]:

$$R_s = (\varepsilon_a /\rho_0)^{1/5} \, \tau_d^{\,2/5}, \qquad (1)$$

where R_s, is the radius of shock wave front, ε_a, is the laser energy absorbed by a target, ρ_0, is undisturbed water density and τ_d is time delay. Note that numerical evaluations of equation (1) in all diapason of the energies ε_a, indicate on the fact that supersonic expansion of a shock wave is restricted by time interval ~ 100 ns. Just during that time the motion obeys the law of point explosion. After that time the shock wave propagates with small supersonic velocities and rapidly getting a strong acoustic wave moving with the speed of sound in water $a_0 \sim 1.5$ km.sec^{-1} (~ 1.5 μm.ns^{-1}).

The corresponded dynamics is illustrated in the interferograms in Fig. 2(a-c). The interferogram in Fig. 2(a) corresponds to the situation, when the ablation plasma and the shock wave moves together with a supersonic speed.
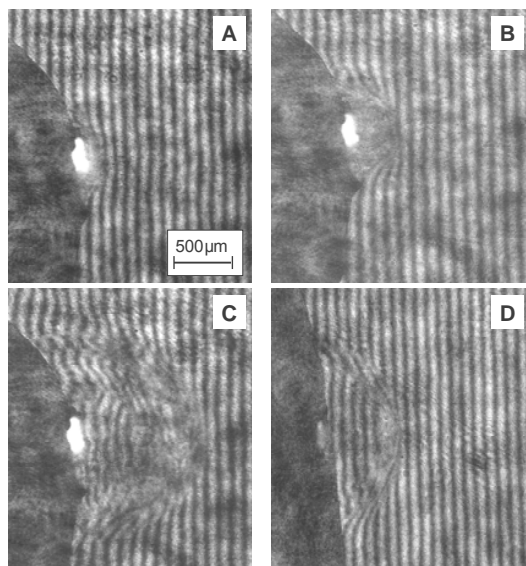

Fig. 2. Interferograms demonstrating dynamics of shock wave in water. A, B, C-laser pulse energy ε_{lp}=75 mJ; D- ε_{lp}=47 mJ. Time delays: A-35; B-153; C-581 and D-484 ns

At time delays longer then ~ 40 ns (see Fig. 2(b)), a shock wave outdistances the ablation plasma and continue to propagate with moderate supersonic velocities. Phase changes of the probing wave of the green light λ=532 nm in the transparent object are too large to be visualized on interferograms in early and mediate moments of time. The phase changes are getting small enough to be visualized in interferograms by visible shifts of the fringes for time delays depending on the absorbed energy ε_a, but longer than ~ 600 ns for $\varepsilon_{lp=}$75 mJ and ~ 450 ns for $\varepsilon_{lp=}$45 mJ . This situation is illustrated in the interferograms 2(c, d).

1.3. Dynamics of interaction

Essential factor of effective generation of a shock wave is well developed process of evaporating a metal surface subject to intensive NIR laser radiation. This phenomenon has the threshold character: it starts after exceeding some critical intensity (flux) of the laser radiation q_c. At smaller intensities the heating the surface layer of a metal leads to propagation of a strong acoustic wave. In special series of experiments the laser pulse energies were varied from $\varepsilon_{lp} = 10$ to 100 mJ. The energies absorbed by the metal target were evaluated from 2.8 to 28 mJ ($q=0.024-0.24$ GW.cm^{-2}). The threshold intensity of the laser radiation has been determined experimentally as $q_c=0.34$ and 0.51 GW.cm^{-2}, for silver and gold correspondently. For larger intensities the process of the developed evaporation of a metal surface is getting more pronounced that leads to quick enhancing the shock wave velocity. It is interesting to remark that at intensities of the NIR radiation higher than $q_{lp} \sim 1.0-1.2$ GW.cm^{-2}, water starts to breakdown volumetrically in the vicinity of a target (see [7]) and is effectively heated by the radiation. This effect is getting visible on interferograms.

The interferometric pictures presented in Fig. 2 illustrate different stages of the expansion dynamics of high temperature surface plasma, which generates a strong shock wave in the surrounding liquid under conditions of the well developed vaporization. If the shock wave moves with supersonic velocities the process of extension may be approximated by the law of point explosion as it is seen in Fig. 3(a), where dynamics of shock wave is shown in early moment of time up to τ_d =50 ns. At time delays $\tau_d \leq 40$ ns the shock wave front propagates together with the ablation plasma. At longer delays, the front continues its motion with supersonic velocities outdistances the contact boundary between ablation plasma and water. After this time the plasma rapidly decelerates its motion. Approximately this moment of time is illustrated by the interferogram in Fig. 2(b). The detached spherical shock wave also rapidly diminishes its speed and moves with moderate supersonic speeds. For time delays longer than ~ 80 ns the shockwave asymptotically moves with the sonic speed in water $a_0 \sim 1.5$ km/sec. In some respects the dynamics of the plasma-shock wave complex reminds the process of the volumetric water breakdown accurately described in [7] for cavities, which arise due to inclusion particles in water.
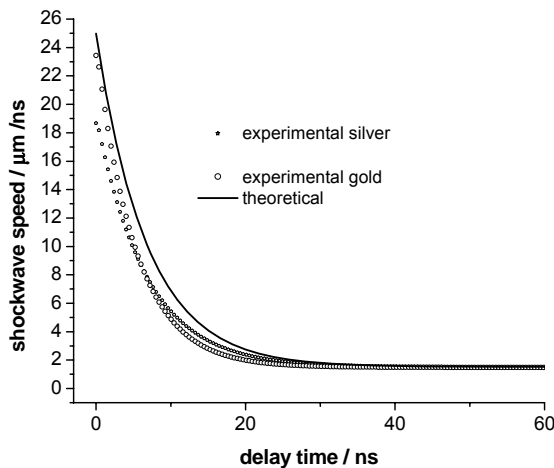
Fig. 3. Speed dynamics of shock wave in water

Supersonic dynamics of the spherical shock wave in water can be compared with the theoretical dependence (1). In Figure 3 it is seen the three graphs: graphical dependences of the velocity $dR_s/dt=D_s$ of a shock wave obtained experimentally as a function of time delay for $\varepsilon_{lp}=75$ mJ, for silver and gold targets; and dependence of velocity D_s on τ_d in accordance with Equation (1) for absorbed energy $\varepsilon_{a=}115$ mJ. The graphical dependences show that real expansion of the laser plasma cannot be approximate by the point explosion in water in accordance with [6]. It seems that when the expansion of the point object realizes in semi-space and, taking into account finite size of the focal spot, the shock wave propagates with enhanced velocities in comparison with the case of spherical expansion of point explosion.

1.4. Evaluation of thickness of the compressed layer of water and pressure behind the front of a shock wave

Interference measurements show that ablation plasma between compressed shock layer of water and the target surface consists of two regions in axial direction: (*) a dense surface laser plasma attached to the surface of the target, and (**) rarified plasma (plus may be water vapors), existing between the dense plasma and the contact boundary of laser plasma and compressed water.

The picture of the radial distribution of the density behind the front of a shock wave may be calculated by reducing interferogram obtained for longer moments of time on the base of averaged data. It is connected with the fact that the shock layer of water cannot be calculated from an interferogram. The case is that the thickness and amplitude of compression of the layer of water are hardly can be evaluated, first, because of a finite distance which shock wave travels during the probing pulse, i.e. the shock wave front will be blurred on the imaged (see Fig. 2(c, d)), and second, due to the very thin compressed layer of water (~micron), shorter

than spatial resolution of the method. The thickness and amplitude of compression of water in the shock layer can be found taking into account physical parameters of the process.

The pressure behind the shock wave in water and linearized hydrodynamic parameters, when $P_s \leq 1$ kbar, are connected by semi-empirical expression [8]:

$$P=(1/m)\rho_0 M_s^2 a_0^2(1-1/M),\qquad(2)$$

Where $M_s=D_s/a_0,$ is the Mach number of a shock wave, $m=2.1$. On the other hand, index of refraction in shock compressed water and pressure are correlated as:

$$P=\rho_0 M_s^2 a_0^2 \Delta n/0.33\qquad(3)$$

Thus the refraction index depends on M_s as:

$$\Delta n=0.33/m(1-1/M_s).\qquad(4)$$

The value of the interference fringe shift on a shock front may be described as: $k=\Delta nL/\lambda$, where L is the distance of traveling the probing beam in the compressed water, λ is its wavelength. The length L, can be expressed through the thickness δ, of the layer of water, and finely is written as:

$$\delta=1/8R_s(k\lambda/\Delta n)^2.\qquad(5)$$

Thus, knowing the fringe shift k, and experimentally obtained dependence (see Fig.3) of the Mach number and radius of the shock wave, the thickness of the compressed layer can be easily evaluated from equation (5).

For the interferogram imaged in Fig. 2(d): $k=5$, $M_s=1.12$, $R_s=0.756$ mm and $\Delta n=1.68.10^{-2}$ the thickness of the compressed layer of water is equal to ~ 4 μm ; for interferogram 2(c): $k=3$, $M_s=1.08$, $R_s=0.945$ mm and $\Delta n=1.16.10^{-2}$ $\delta=2.5$ μm. Correspondent pressures behind the front of shock wave were evaluated in accordance with (2) (or (3)) as ~ 1.4 and 0.92 kbar.

The pressures behind the front of a shock wave in water can be evaluated for earlier moments of time interaction of the NIR laser radiation with a metal target. For this purpose can be analyzed the data given in [8], where pressures depend on Mach numbers of the shock in water. For mediate values of Mach numbers $M_s \approx 5$, when a shock wave outdistances the contact boundary between ablation plasma and water, the pressure is evaluated as $P_s \sim 0.3$ Mbar. For maximal values $Ms \approx 12$ the pressure can be evaluated as of the order of $P_s \sim 3$ Mbar.

II. CONCLUSION

The underwater processes of the NIR laser beam-metal target interaction were visualized and measured by applying Mach-Zehnder interference technique. The picture of the transparent object was imaged on the CMOS sensor of a full-frame camera with the spatial resolution of *24* microns. The

model of hydrodynamics of laser-target interaction was proposed for the focused beam of *1064* nm Nd:YAG laser radiation and a metal (silver and gold) target in water. The values of critical intensities of the NIR radiation for developed vaporization of silver and gold targets were measured experimentally. Obtained interferograms allowed evaluating the thickness of the water layer compressed by the shock and the pressure behind its front.

REFERENCES

[1] S. Siano, R. Pini, R. Salimbeni, M. Vannini,"Imaging and analysis of photomechanical effects induced in water by high-power laser-target interaction," Appl. Phys. B 62, pp. 503-510 (1996)

[2] T. G. Jones, J. Grun, L. D. Bibee, C. Manka, A. Landsberg, D.Tam,"Laser-generated shocks and bubbles as laboratory-scale models of underwater explosions," Shock and Vibration, V.10, No. 3, pp. 147-157, (2003)

[3] P.V. Kazakevich, A.V. Simakin, V.V. Voronov, G.A. Shafeev,"Laser induced synthesis of nanoparticles in liquids,"Applied Surface Science 252, pp. 4373–4380 (2006)

[4] M. Bereznai, P. Heszler b,c, Z. To, O. Wilhelmsson, M. Boman, "Measurements of nanoparticle size distribution produced by laser ablation of tungsten and boron-carbide in N2 ambient,"Applied Surface Science 252, pp. 4368–4372 (2006)

[5] G.V. Dreiden, Y.I. Ostrovsky, I.V. Semenova in Proc. Holographic International '92, SPIE Vol. 1732, pp.651-656.

[6] L.I. Sedov, *"Similarity and dimensional methods in mechanics"*, Mir Publishers (1982).

[7] G. Toker, V. Bulatov, T. Kovalchuk and I. Schechter, "Micro-Dynamics of Optical Breakdown in Water Induced by Nanosecond Laser Pulses of 1064 nm Wavelength,"Chemical Physics Letters 471, pp. 244–248 (2009)

[8] Y.S. Yakovlev, "Hydrodynamics of explosion", Sudpromgiz, Leningrad (1961)

G.R. Toker (MS-74–PhD-88) was graduated at the Moscow Institute of Physics and Technology and earned his PhD degree in 1988 at the Moscow Institute of General Physics. More then 40 article and reports are published in international journals and conferences on optical diagnostics of phase object by methods of holographic and classic interferometry. Now Research Professor at the Israel Institute of Technology